Biofilm Growth Under Elastic Confinement

George T. Fortune[1], Nuno M. Oliveira[1,2], and Raymond E. Goldstein[1]
[1] *Department of Applied Mathematics and Theoretical Physics, Centre for Mathematical Sciences, University of Cambridge, Wilberforce Road, Cambridge CB3 0WA, United Kingdom*
[2] *Department of Veterinary Medicine, University of Cambridge, Madingley Road, Cambridge CB3 0ES, United Kingdom*
(Dated: December 6, 2021)

Bacteria often form surface-bound communities, embedded in a self-produced extracellular matrix, called biofilms. Quantitative studies of their growth have typically focused on unconfined expansion above solid or semi-solid surfaces, leading to exponential radial growth. This geometry does not accurately reflect the natural or biomedical contexts in which biofilms grow in confined spaces. Here we consider one of the simplest confined geometries: a biofilm growing laterally in the space between a solid surface and an overlying elastic sheet. A poroelastic framework is utilised to derive the radial growth rate of the biofilm; it reveals an additional self-similar expansion regime, governed by the stiffness of the matrix, leading to a finite maximum radius, consistent with our experimental observations of growing *Bacillus subtilis* biofilms confined by PDMS.

Bacterial biofilms are microbial accretions, enclosed in a self-produced polymeric extracellular matrix [1], which adhere to inert or living surfaces. A biofilm gives the individual cells a range of competitive advantages, such as increased resistance to chemical attack. Since the popularisation in the mid 1600s of the light microscope as a tool to study problems in biology [2, 3], observations of groups of bacteria on surfaces have been amply documented [4], most notably by van Leeuwenhoek in his dental plaque [5]. Yet, it is only in the last few decades with the development of new genetic and molecular techniques that the complexity of these communities has been appreciated and biofilm formation has been recognised as a regulated developmental process in its own right [6, 7].

Biofilm formation is common across a wide range of organisms in the archaeal and bacterial domains of life, on almost all types of surfaces [8]. Cells attach to a surface and form micro-colonies through clonal growth. These then grow and colonise their surroundings through twitching motility [1]. A central research focus has been understanding these growth dynamics. Building on important work on osmotically-driven spreading [9], a biofilm has often been modelled as a viscous, Newtonian fluid mixture (nutrient rich water and biomass), neglecting the matrix elasticity. The effects of surface tension [10], osmotic pressure [11], and the interplay between nutrients, cell growth, and electrical signaling in response to metabolic stress have all been studied recently [12].

While previous analyses have focused on the experimentally tractable cases of unconfined and unsubmerged biofilms [9–12], they do not accurately reflect the conditions in which many biofilms grow; they thrive in confined micro-spaces [13] between flexible elastic boundaries such as vessel walls or soil pores [14], and indeed in the human body, where they account for over 80% of microbial infections [15]. Biofilms are difficult to treat with antibiotics, being thousands of times more resistant than the constituent microorganisms in isolation [16] due to a range of mechanical and biological processes [17, 18]. The recent rapid growth in the use of implantable biomedical devices (stents, catheters, and cardiac implants) has brought with it a large increase in associated biofilm infections [19] since artificial surfaces require much smaller bacterial loads for colonisation than the corresponding volume of native tissue ($\approx 10^{-4}$ as much [20]).

Here we develop the simplest model for a confined biofilm, using a poroelastic framework to obtain a system of equations describing its expansion dynamics. We find an analytic similarity solution for the biofilm height and radius, together with the vertically averaged biomass volume fraction. Consistent with experimental observations on growing *Bacillus subtilis* biofilms described here, unlike unconfined biofilms whose radius grows exponentially, the balance between elastic stresses and osmotic pressure difference across the interface implies an additional possible growth regime where within a shal-

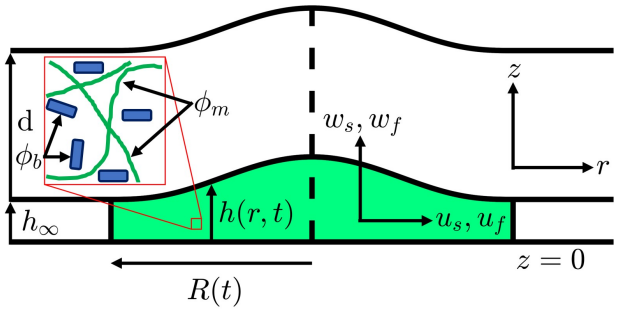

FIG. 1. Schematic of a confined biofilm. An axisymmetric biofilm (green) grows between a rigid surface at $z = 0$ and an elastic sheet at $z = h$, with undeformed gap height h_∞. Inset: the biomass is a mixture of bacterial cells (blue, volume fraction ϕ_b) and extracellular matrix (green,volume fraction ϕ_m). The pore-averaged velocities of the solid and fluid phases are denoted by $\boldsymbol{u_s} = (u_s, w_s)$ and $\boldsymbol{u_f} = (u_f, w_f)$.

low layer lubrication assumption, confined biofilms have a maximum radius at long times. The transition between regimes is governed by the stiffness of the matrix.

We consider a bio-mechanical system in which bacteria grow and divide, converting nutrient-rich fluid into biomass and thus inducing a flow of biomass outwards from the biofilm centre. This flow is resisted by elastic stresses within the extracellular matrix (ECM), while the biofilm height dynamically adjusts to ensure conservation of normal stress across the overlying elastic sheet. An influx of water assures volume conservation. Illustrated in Fig. 1, an axisymmetric biofilm of thickness $h(r,t)$, radius $R(t)$ and biomass volume V rests on an impermeable flat plate at $z=0$ and grows below an elastic sheet of thickness $d=\mathcal{O}(R)$ and bending modulus $B=Ed^3/12(1-\nu^2)$, where E and ν are the Young's modulus and Poisson's ratio of the sheet. We examine the simplest biofilm composition, a mixture of bacteria (volume fraction ϕ_b), sugar-rich secreted polymeric ECM (volume fraction ϕ_m), and nutrient-rich water (modelled as a low viscosity Newtonian fluid [9] with dynamic viscosity μ_f and volume fraction $1-(\phi_m+\phi_b)\equiv 1-\phi$), under the assumption that $\phi_m \ll \phi_b$ [9]. For theoretical simplicity, we assume that the biomass volume fraction ϕ is independent of z, so $\partial\phi/\partial z=0$.

We denote the pore-averaged velocity and stress tensor of the solid and liquid phases by $\{\boldsymbol{u_s}=(u_s,w_s)\,,\,\boldsymbol{\sigma_s}\}$ and $\{\boldsymbol{u_f}=(u_f,w_f)\,,\,\boldsymbol{\sigma_f}\approx -p\boldsymbol{I}\}$ [9] respectively, where p, Π and $\tilde{p}$ are the pore, osmotic, and bulk pressures (with $\tilde{p}=p+\Pi$ [21]). Since the vertical deflection of the sheet $\Delta d=\mathcal{O}(h)$ is small compared to its thickness d, we ignore stretching and model it as a thin elastic beam with radius of curvature $\tilde{R}\gg\{d,\,h\}$ and surface tension γ against the biofilm. We neglect gravity, assume that nutrient concentrations across the biofilm are constant, and take the biomass growth rate g to have the saturating form

$$g=\frac{1}{T_D}\left(\frac{c}{c+c_{\text{half}}}\right), \tag{1}$$

independent of position, where T_D is the doubling time (typically hours), c is the concentration of a limiting nutrient and c_{half} is that for half-maximum growth rate. Both c and hence g are taken to be constant in light of our experiments, introduced below, in which there is an external flow that ensures homogeneity. Conserving mass in both the solid and fluid phases gives

$$\frac{\partial\phi}{\partial t}+\boldsymbol{\nabla}\cdot(\phi\boldsymbol{u_s})=g\phi, \tag{2a}$$

$$-\frac{\partial\phi}{\partial t}+\boldsymbol{\nabla}\cdot((1-\phi)\boldsymbol{u_f})=-g\phi. \tag{2b}$$

Defining the Terzaghi effective stress tensor as $\boldsymbol{\sigma}=\phi(\boldsymbol{\sigma_s}-\boldsymbol{\sigma_f})$ [22], momentum balance yields

$$\boldsymbol{\nabla}\cdot\boldsymbol{\sigma}=\boldsymbol{\nabla}p. \tag{3}$$

To model $\boldsymbol{\sigma}$, we deviate from prior work that assumed a Newtonian fluid by adopting a poroelastic framework that incorporates the elasticity of the ECM. In this picture, $\boldsymbol{\sigma}$ obeys the elastic constitutive law

$$\sigma=\sigma\left(\boldsymbol{\nabla\xi}\right), \tag{4}$$

where $\boldsymbol{\xi}=(\xi,\zeta)$, the deformation vector of the medium away from a reference state, is related to the biofilm phase velocity through $\boldsymbol{u_s}=(\partial_t+\boldsymbol{u_s}\cdot\boldsymbol{\nabla})\,\boldsymbol{\xi}$. Little utilised in the study of biofilms, it is a common approach in many problems containing elasticity in geophysics (hydrology subsidence and pumping problems [23, 24] or industrial filtration [25]) and biological physics (cell cytoplasm [26]). Here, we consider the simplest case, where $\boldsymbol{\sigma}$ obeys the linear constitutive law

$$\boldsymbol{\sigma}(\boldsymbol{\nabla\xi})=\left(K-\frac{2G}{3}\right)(\boldsymbol{\nabla}\cdot\boldsymbol{\xi})\boldsymbol{I}+G(\boldsymbol{\nabla\xi}+\boldsymbol{\nabla\xi}^T), \tag{5}$$

where K and G are the effective bulk and shear moduli of the biofilm respectively, assumed constant. As in [23], K and G are properties of the whole biofilm rather than just the ECM. We prescribe explicitly the general form for the horizontal velocity of the solid phase,

$$u_s=\frac{r}{R}\frac{\partial R}{\partial t}u_0\left(\frac{z}{h}\right), \tag{6}$$

where u_0 is the $z-$dependent part of u_s. We take

$$u_0=\frac{6z(h-z)}{h^2}, \tag{7}$$

since this is the simplest functional form obeying no-slip boundary conditions at $z=0$ and $z=h$ as well as $\langle u_0\rangle=1$. However, as shown below, we find a solution independent of the exact form for u_0. Global volume conservation gives $\partial R/\partial t$ while r/R sets a simple linear radial dependence, ensuring that $u_s=0$ at $r=0$. As for u_0, tweaking this radial dependence does not qualitatively change the resulting dynamics of the system.

In contrast, vertical flow is governed by pressure gradients induced both by the upper confinement and by elastic stresses in the extracellular matrix. We invoke Darcy's law for flow within the matrix, giving

$$(1-\phi)(w_s-w_f)=\frac{\kappa}{\mu_f}\frac{\partial p}{\partial z}. \tag{8}$$

where $\kappa=\kappa(\phi)$ is the effective biofilm permeability with characteristic permeability scale κ_0. The osmotic pressure away from equilibrium $\Pi(\phi)$ is taken to be that of Flory Huggins theory [27], with interaction parameter $\chi\simeq 1/2$ so there is no demixing [28]. Assuming that the matrix solid fraction $\beta=\phi_m/\phi\ll 1$ is constant across the biofilm, the osmotic pressure is [29]

$$\Pi=\frac{k_BT}{3\nu_0}\left(\frac{\phi_m}{1-\phi}\right)^3, \tag{9}$$

a function of thermal energy k_BT and ν_0, the effective volume occupied by one monomer of matrix. Since the matrix consists of many different substances, notably sugars, proteins and DNA, we estimate ν_0 by the volume occupied by one sugar monomer. This term is subdominant in the analysis below, and thus does not appear in the interior ($r \leq R$) solutions (14) - (18). We close this system of equations with a set of vertical boundary conditions, given in the Supplementary Material [30].

The analysis exploits two separations of scales: (i) the initial radius of the confined biofilm $R_0 = R(t = 0)$ is much greater than the initial height $H_0 = h(r = 0, t = 0)$, a lubrication approximation, and (ii) the growth time scale $1/g$ is much larger than the poroelastic equilibration time $\mu_f H_0^2/\kappa_0 P_0$. We nondimensionalise the equations anisotropically using these length scales, denote the vertically averaged form of a function f by $\langle f \rangle = h^{-1}\int_0^h f\, dz$, and define $\varphi = \langle \phi \rangle$, $v_s = \langle u_s \rangle$, $k = \langle \kappa \rangle$, $\mathcal{P} = p/P_0$ and

$$\rho = \frac{r}{R(0)}, \quad \tau = gt, \quad \mathcal{R} = \frac{R(t)}{R(0)}, \quad \mathcal{H} = \frac{h(r,t)}{h(0,0)}. \tag{10}$$

Keeping only leading-order terms in $\epsilon = H_0/R_0$ [30], the model reduces to coupled PDEs for the height $\mathcal{H}(\rho, \tau)$ and depth-averaged biomass fraction $\varphi(\rho, \tau)$ as functions of radial distance ρ and time τ. The horizontal pressure gradient adjusts to one of three possible modes

$$\frac{\partial \mathcal{P}}{\partial \rho} = \left\{0, \frac{C_1}{\rho}, \frac{C_2}{\rho^2}, \right\} \tag{11}$$

where C_1 and C_2 are constants and the dominant contribution to the pressure $\mathcal{P}$ arises from the bending stresses imposed from the upper elastic sheet,

$$\mathcal{P} = \nabla^4 \mathcal{H}. \tag{12}$$

The depth-integrated biomass fraction $\varphi\mathcal{H}$ satisfies a conservation law of the form $\partial(\varphi\mathcal{H})/\partial\tau = -\boldsymbol{\nabla}\cdot\boldsymbol{\mathcal{J}}_\varphi + \boldsymbol{\mathcal{S}}$,

$$\frac{\partial}{\partial\tau}(\varphi\mathcal{H}) = -\frac{1}{\rho}\frac{\partial}{\partial\rho}\left(\rho v_s \varphi\mathcal{H}\right) + \varphi\mathcal{H}. \tag{13}$$

Thus, $\varphi\mathcal{H}$ grows exponentially from the source term $\boldsymbol{\mathcal{S}} = \varphi\mathcal{H}$, while subject to radial advection at speed $v_s(\mathcal{H}, \mathcal{R})$ from the flux term $\boldsymbol{\mathcal{J}}_\varphi$. The system is closed with a set of boundary conditions, deriving the boundary conditions for $\mathcal{H}$ at the biofilm interface by extending the framework outside the biofilm to the whole domain and imposing far field boundary conditions [30]. In the mode zero case when the horizontal pressure gradient is zero, Eqs. (11)-(13) admit the interior ($\rho \leq \mathcal{R}$) solutions

$$\mathcal{H} = e^{\tau}\mathcal{R}^{-2} f(\rho/\mathcal{R}), \tag{14a}$$
$$\varphi_0 = \varphi_0(\rho/\mathcal{R}), \tag{14b}$$

where

$$f(x) = 1 - (1 - m_0)\, x^2, \tag{15}$$

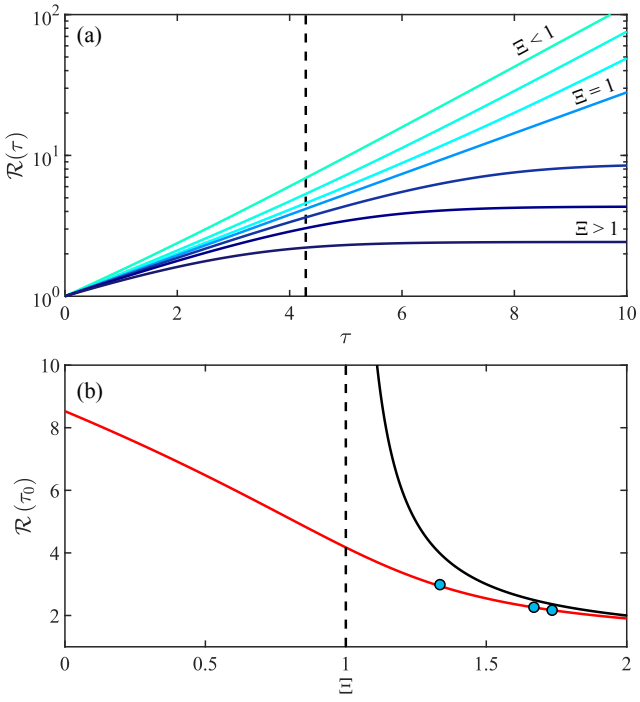

FIG. 2. Growth dynamics of confined biofilms according to the poroelastic model. (a) The scaled biofilm radius $\mathcal{R}$ as a function of scaled time in a semilogarithmic plot, for $\Xi \in [0.4, 0.75, 0.91, 1, 1.13, 1.3, 1.7]$. Darker colours denote larger Ξ. (b) Biofilm radius at a fixed τ_0 (dashed vertical line in (a)) as a function of Ξ, both numerically (-) and experimentally (•), and numerically for $\tau_0 \to \infty$ (-).

the incline ratio

$$m_0 = \frac{h(r = R(0), t = 0)}{h(r = 0, t = 0)} \tag{16}$$

is a measure of the initial flatness of the biofilm, $\varphi_0(\rho) = \varphi(\rho, \tau = 0)$ is set from the initial conditions and we have utilized the vertically-averaged boundary conditions [30] and the initial conditions $\mathcal{H}(\rho = 0, \tau = 0) = \mathcal{R}(\tau = 0) = 1$ and $\mathcal{H}(\rho = 1, \tau = 0) = m_0$. The form of (14) guarantees that the total biomass $\int d\rho\rho\, \mathcal{H}\varphi$ grows as e^{τ}. We obtain $\mathcal{R}(\tau)$ as the solution of the cubic equation

$$e^{-\tau}\mathcal{R}^3 + \mathcal{R}(\Xi - 1) - \Xi = 0, \tag{17}$$

where the single free parameter is

$$\Xi = \frac{\xi_0 m_0}{\zeta_0}\frac{K + G/3}{K + 4G/3} = \frac{\Psi}{2(1 - \nu_b)}. \tag{18}$$

Derived in [30], $\Psi = \xi_0 m_0/\zeta_0$ is a measure of the initial ratio between horizontal and vertical stress gradients in the biofilm while ν_b, the effective Poisson's ratio of the ECM, is a measure of how stiff the biofilm is (stiffer biofilms have lower ν_b). The radial expansion of the biofilm is mediated by a balance at the biofilm edge between horizontal and vertical elastic deformation in the

biofilm (the Ξ and $e^{-\tau}\mathcal{R}^3$ terms, respectively, in (17)) and the osmotic pressure difference across the biofilm interface (the $\mathcal{R}(\Xi-1)$ term).

For general Ξ and τ, this equation does not always admit an analytic solution and is solved numerically [30]. Figure 2(a) plots the temporal evolution of $\mathcal{R}$ for a range of different values of Ξ. Figure 2(b) explores this further, choosing a fixed observation time τ_0 and plotting $\mathcal{R}(\tau_0)$ as a function of Ξ. Two clear regimes emerge. If $\Xi < 1$, the first and second terms in (17) dominate in a balance between stresses caused by the vertical elastic deformations and the osmotic pressure difference, leading to a limit on vertical expansion. The biofilm then spreads with exponential radial growth [9], with $\mathcal{R} \to (1-\Xi)^{1/2}\, e^{\tau/2}$ as $\tau \to \infty$. If $\Xi > 1$ (the dark blue curves in figure 2(a)), the second and third term in (17) are dominant, giving a balance between stresses caused by horizontal elastic deformations and the osmotic pressure difference that limits horizontal expansion. The radius at intermediate times exhibits power-law growth before slowing down to reach a maximum $\mathcal{R}(\infty) = \Xi/(\Xi-1)$, when the shallow layer approximation is still valid. In the special case $\Xi = 1$, the osmotic pressure difference across the interface is zero, leading to a balance between horizontal and vertical elastic stresses. As shown in Fig. 2(a), the system exhibits transitional exponential growth, with $\mathcal{R} = e^{\tau/3}$, but this state is not stable; curves with Ξ just above and below unity will veer off eventually to tend to a constant radius or to the faster $e^{\tau/2}$ growth law.

We performed experiments on the growth of biofilms confined by polydimethylsiloxane (PDMS), the results of which can be compared directly to the model developed above. The methodology follows existing protocols [12, 31, 32] developed to understand the growth of focal (and submerged) biofilms under well-defined flow conditions. Full details are given in Supplemental Material [30]; here we summarize the key features. Flagella-less mutants of *Bacillus subtilis* were used to avoid secondary contributions to biofilm spreading [9]. Cells in exponential growth phase were centrifuged and resuspended in growth medium before being loaded at the centre of Y04-D plates linked to the CellASIC ONIX microfluidic platform (EMD Millipore), and kept at 30 °C. In this setup, they are confined between glass and an overlying PDMS sheet of thickness $d = 114\,\mu$m, with an initial gap of $h = 6$ μm. Fresh medium was flowed through the chamber with a mean speed of $\sim 16\,\mu\text{ms}^{-1}$ [12, 31, 32]. Biofilm growth was imaged at 1 frame/minute on a spinning-disc confocal microscope in bright field. As the biofilms were often frilly, with long thin strands of matrix polymer protruding from their edges, a Gaussian image processing filter in MATLAB was used to neglect these strands when identifying the interface with a Sobel edge detector.

Figure 3(a) is a montage of the expanding biofilm edge and the best-fit circle for one particular experiment, while Figure 3(b) plots the scaled biofilm radius $\mathcal{R}$ as a function of time. In a clear departure from unconfined bacterial biofilms, the $\mathcal{R}$ initially grows as a power law before tending to saturate at long times. These profiles exhibit the main qualitative features predicted by the theoretical model for $\Xi > 1$. The lines of best fit (black lines in 3(b), [30]) show good agreement over the entire time course of the experiments. A further comparison with theory is obtained by measuring in three different experiments, at the same nutrient concentration, the radius $\mathcal{R}(t_0)$ at a particular time $t_0 = 5\,$h, chosen as a time when the biofilm radius had a least doubled from its initial value. The parameter g relating absolute and rescaled times was fitted across all experiments, and gives the value $\tau_0 = 4.29$ used in Fig. 2(b), while Ξ is fitted independently for each. These experimental points in the $\Xi - \mathcal{R}$ plane are shown as blue circles in Figure 2b), and agree very well with the poroelastic model developed here.

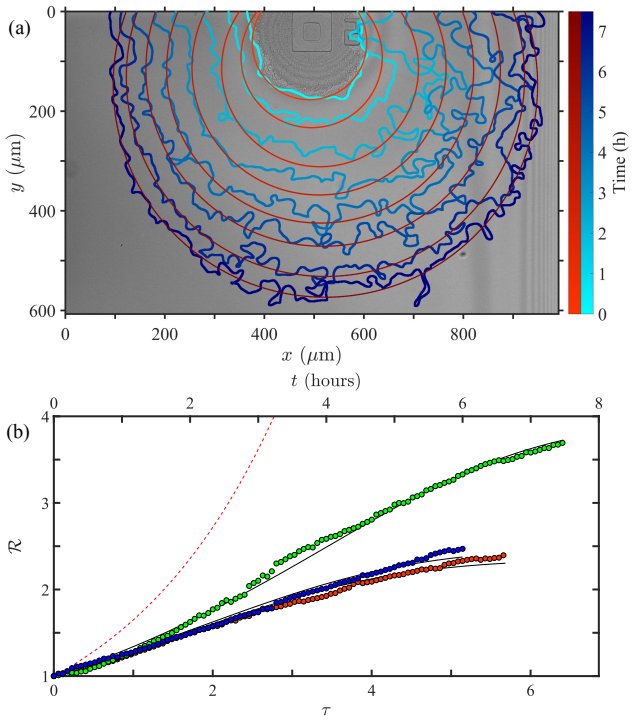

FIG. 3. Experimental growth of *B. subtilis* biofilms under confinement by a PDMS sheet. (a) Montage plot, superimposed on image of the initial biofilm, showing the temporal evolution of the biofilm boundary (blue curves; darker colors denote later times) and fitted circles (red). (b) Scaled biofilm radius $\mathcal{R}$ against scaled time for 3 experiments (● , ● , ●) compared to fitted dynamics from model (–) Dashed red curve is $\mathcal{R}(\tau) = \mathrm{e}^{\tau/2}$ expected for growth at constant thickness.

Motivated by the desire to understand the evolution of biofilms under confinement, we have constructed a minimal mathematical model that uses a poro-elastic framework. This admits a family of self-similar quasi-steady solutions, parameterized by a dimensionless parameter Ξ that measures the elasticity of the matrix. Those so-

lutions are consistent with the experimentally observed behavior of confined *B. subtilis* biofilms. For comparison, [30] presents the corresponding theoretical model in which, following previous work in the literature, the biomass is modelled instead as a viscous Newtonian fluid, neglecting the intrinsic elasticity of the biofilm ECM. In that case, a solution with power law growth tending to a maximum finite biofilm radius is not supported, demonstrating that modelling the matrix elasticity is essential to capturing biofilm growth under elastic confinement.

Unlike unconfined biofilms, a subset of these solutions (where $\Xi > 1$) have a maximum radius due to a balance between elastic stresses and the osmotic pressure difference across the interface. The key parameter that determines which regime the system lies in and thus whether the biofilm grows predominately radially or axially is the stiffness of the biofilm matrix. Hence, we may view matrix elasticity is a competitive trait that could well be optimized by natural selection.

We are grateful to G.G. Peng and J.A. Neufeld for discussions and P.A. Haas and A. Chamolly for valuable comments on an earlier version of the manuscript. This work was supported in part by the Engineering and Physical Sciences Research Council, through a Doctoral Training Fellowship (GTF) and an Established Career Fellowship EP/M017982/1 (REG), and by a Wellcome Trust Interdisciplinary Fellowship and Discovery Fellowship BB/T009098/1 from the Biotechnology and Biological Sciences Research Council (NMO).

[1] T. Bjarnsholt, Introduction to biofilms, in *Biofilm Infections*, T. Bjarnsholt, P.Ø. Jensen, C. Moser and N. Høiby, eds. (Springer, New York, 2011), pp. 1-9.

[2] R. Hooke, Micrographia, or, Some physiological descriptions of minute bodies made by magnifying glasses :with observations and inquiries thereupon, London : Printed by J. Martyn and J. Allestry, printers to the Royal Society (1665)

[3] P. G.Saraf, A. T. K. Cockett, Marcello Malpighi — A Tribute, Urology **23**, 619-623 (1984)

[4] J. Wimpenny, W. Manz, U. Szewzyk, Heterogeneity in biofilms, FEMS Microbiol. Rev. **24**, 661 (2000).

[5] A. van Leeuwenhoek, An abstract of a letter from Mr. Anthony Leewenhoeck at Delft, dated Sep. 17. 1683. Containing some microscopical observations, about animals in the scurf of the teeth, the substance call'd worms in the nose, the cuticula consisting of scales, Phil. Trans. R. Soc. **14**, 568 (1684).

[6] J. W. Costerton, Z. Lewandowski, D. Debeer, D. Caldwell, D. Korber, G. James, Biofilms, the Customized Microniche, J Bacteriol. **176**, 2137 (1994).

[7] G. O'Toole, H. B. Kaplan, R. Kolter, Biofilm formation as microbial development, Annu. Rev. Microbiol. **54**, 49-79 (2000)

[8] D. López, H. Vlamakis, and R. Kolter, Biofilms, Cold Spring Harb. Perspect. Biol. **2**, a000398 (2010).

[9] A. Seminara, T.E. Angelini. J.N. Wilking, H. Vlamakis, S. Ebrahim, R. Kolter, D.A. Weitz, and M. P. Brenner, Osmotic spreading of *Bacillus subtilis* biofilms driven by an extracellular matrix, Proc. Natl. Acad. Sci. USA **109**, 1116 (2012).

[10] A. Tam, E.F. Green, S. Balasuriya, E.L. Tek, J.M. Gardner, J.F. Sundstrom, V. Jiranek, and B.J. Binder, A thin-film extensional flow model for biofilm expansion by sliding motility, Proc. R. Soc. A **475**, 20190175 (2019).

[11] S. Srinivasan, C.N. Kaplan, and L. Mahadevan, A multiphase theory for spreading microbial swarms and films, eLife **8**, e42697 (2019).

[12] R. Martinez-Corral, J. Liu, A. Prindle, G. M. Süel, and J. Garcia-Ojalvo, Metabolic basis of brain-like electrical signalling in bacterial communities, Phil. Trans. R. Soc. B **374**, 20180382 (2019).

[13] F. Kempf, R. Mueller, E. Frey, and J. M. Yeomans, Active matter invasion, Soft Matter **15**, 7538 (2019).

[14] J. C. Conrad and R. Poling-Skutvik, Confined Flow: Consequences and implications for bacteria and biofilms, Annu. Rev. Chem. Biomol. Eng. **9**, 175 (2018).

[15] Z. Khatoon, C.D. McTiernan, E.J. Suuronen, T.-F. Mah, and E. I. Alarcon, Bacterial biofilms formation on implantable devices and approaches to its treatment and prevention, Heliyon **4**, 1 (2018).

[16] Y. Oppenheimer-Shaanan, N. Steinberg, and I. Kolodkin-Gal, Small molecules are natural triggers for the disassembly of biofilms, Trends Microbiol. **21**, 594 (2013).

[17] O. Ciofu, E. Rojo-Molinero, M.D. Macià, and A. Oliver, Antibiotic treatment of biofilm infections, APMIS **125**, 304 (2017).

[18] P. S. Stewart, Mechanisms of antibiotic resistance in bacterial biofilms, Int. J. Med. Microbiol. **292**, 107 (2002).

[19] C. R. Arciola, D. Campoccia, and L. Montanaro, Implant infections: adhesion, biofilm formation and immune evasion, Nat. Rev. Microbiol. **16**, 397 (2018).

[20] J. Nowakowska, R. Landmann, and N. Khanna, Foreign body infection models to study host-pathogen response and antimicrobial tolerance of bacterial biofilms, Antibiotics **3**, 378 (2014).

[21] S.S.L. Peppin, J.A.W. Elliott, and M. G. Worster, Pressure and relative motion in colloidal suspensions, Phys. Fluids **17**, 053301 (2005).

[22] H.F. Wang, *Theory of Linear Poroelasticity with Applications to Geomechanics and Hydrogeology* (Princeton University Press, Princeton, 2001).

[23] D.R. Hewitt, J.A. Neufeld, and N.J. Balmforth, Shallow, gravity-driven flow in a poro-elastic layer, J. Fluid Mech. **778**, 335 (2015).

[24] R.E. Gibson, R.L. Schiffman, and S.L. Pu, Plane strain and axially symmetric consolidation of a clay layer on a smooth impervious base, Q. J. Mech. Appl. Maths **23**, 505 (1970).

[25] S.I. Barry, G.N. Mercer, and C. Zoppou, Deformation and fluid flow due to a source in a poro-elastitc layer, Appl. Math. Model. **21**, 681 (1997).

[26] G.T. Charras, T.J. Mitchison, and L. Mahadevan, Animal cell hydraulics, J. Cell Sci. **122**, 3233 (2009).

[27] P.J. Flory, *Principles of Polymer Chemistry* (Cornell University Press, Ithaca, 1953).

[28] H.F. Winstanley, M. Chapwanya, M.J. McGuinness, and A.C. Fowler, A polymer-solvent model of biofilm growth, Proc. R. Soc. A **467**, 1449 (2011).

[29] Note that due to the dead volume occupied by the bacte-

ria cells, the extracellular matrix occupies a volume ϕ_m within a total volume of $1-\phi$ and thus we expand in terms of $\phi_m/1-\phi$ rather than ϕ_m.

[30] See Supplemental Material at http://link.aps.org/supplemental/10.1103/XXX for further theoretical details and experimental methods, which includes Refs. 31-36.

[31] J. Liu, A. Prindle, J. Humphries, M. Gabalda-Sagarra, D.D. Lee, S. Ly, J. Garcia-Ojalvo, and G. M. Süel, Metabolic co-dependence gives rise to collective oscillations within biofilms, Nature **523**, 550 (2015).

[32] J. Humphries, L. Xiong, J. Liu, A. Prindle, F. Yuan, H.A. Arjes, L. Tsimring, and G.M. Süel, Species-independent attraction to biofilms through electrical signaling, Cell **168**, 200 (2017).

[33] J. Schindelin, I. Arganda-Carreras, E. Frise, V. Kaynig, M. Longair, T. Pietzsch, S. Preibisch, C. Rueden, S. Saalfeld, B. Schmid, J.-Y. Tinevez, D.J. White, V. Hartenstein, K. Eliceiri, P. Tomancak, and A. Cardona, Fiji: an open-source platform for biological-image analysis, Nature Methods **9**, 676 (2012).

[34] R. P. Brent, *Algorithms for Minimization Without Derivatives* (Prentice-Hall Inc. 1973).

[35] C. Picioreanu, F. Blauert, H. Horn, and M. Wagner, Determination of mechanical properties of biofilms by modelling the deformation using optical coherence tomography, Water Res. **145**, 588-598 (2018).

[36] A.E. Ismail, G.S. Grest, D.R. Heine, and M. J. Stevens, Interfacial Structure and Dynamics of Siloxane Systems: PDMS-Vapor and PDMS-Water, Macromolecules **42**, 3186-3194 (2009).